Received: 11 May 2022 | Revised: 21 June 2022 | Accepted: 8 July 2022

IET Communications

DOI: 10.1049/cmu2.12463

The Institution of Engineering and Technology WILEY

ORIGINAL RESEARCH

Dual pulse shaping transmission with sinc-function based complementary Nyquist pulses

Hang Li[1] | Xiaojing Huang[2] | Jian Andrew Zhang[2] | Hao Zhang[2] | Zhiqun Cheng[1]

[1]School of Electronics and Information Engineering, Hangzhou Dianzi University, Hangzhou, China

[2]Global Big Data Technologies Centre, University of Technology Sydney, Sydney, Australia

Correspondence
Hang Li, School of Electronics and Information Engineering, Hangzhou Dianzi University, Hangzhou 310018, China.
Email: Hangli@hdu.edu.cn

Funding information
National Key R&D Program of China, Grant/Award Number: 2018YFE0207500; Natural Science Foundation of Zhejiang Province, Grant/Award Numbers: LY22F010003, LZ20F010004; National Natural Science Foundation of China, Grant/Award Numbers: 61871169, 62071163; Project of Ministry of Science and Technology, Grant/Award Number: D20011

Abstract

Due to difficulties in manufacturing, data conversion devices with extremely high sampling rate are becoming the bottleneck in realising high-speed communication systems with a large bandwidth. Dual pulse shaping (DPS) transmission allows half-symbol-rate conversion devices to be used for two parallel data streams to achieve full-rate transmission, and is proved to be an effective solution. Here, two sets of ideal sinc-function based complementary Nyquist pulses for DPS transmission are proposed. Theoretically, it is shown that the proposed pulses satisfy the inter-symbol and cross-symbol interference-free conditions, and can achieve full-Nyquist-rate transmission with half of the sampling rate. With reference to commercially available D/As, two sets of practical dual spectral shaping pulses are further proposed, and the close relationship between the ideal and practical pulses are disclosed. Performance analysis for linear equalisation is provided in the presence of both timing offset between dual shaping pulses and carrier-frequency offset. Two approaches are then proposed to improve the system robustness by adjusting the clock phase of the D/As and A/Ds. Simulation results are presented to provide a comparison between the proposed DPS transmission schemes and the state of the art, in terms of the performance metrics of peak-to-average power ratio and bit error rate.

1 | INTRODUCTION

As a fundamental technology in digital single carrier communication systems, Nyquist pulse shaping at the transmitter and matched filtering at the receiver are usually employed to avoid inter-symbol interference (ISI) caused by non-ideal channels and to maximise the signal-to-noise ratio (SNR) of received signals [1]. As a typical family of Nyquist pulses, raised-cosine (RC) pulses are commonly applied in conventional single pulse shaping (SPS) transmission, where the pulse's spectrum satisfies Nyquist's first criterion. Generally, the overall RC spectral characteristic can be split evenly between a root RC (RRC) transmitting filter and an RRC receiving filter. The ratio of the excess bandwidth to the Nyquist frequency, namely the roll-off factor, regulates the practical transmission bandwidth. Given a pulse transmission rate, a smaller roll-off factor always leads to a higher spectral efficiency. However, an RRC filter with very small roll-off factor is extremely difficult to design and implement. Also, it often incurs more serious ISI due to linear distortion during the actual high-speed transmission. Therefore, the improvement on spectral efficiency via reducing the roll-off factor of Nyquist pulse shaping is limited [2]. As a breakthrough of breaking the Nyquist criterion of conventional communication systems, faster-than-Nyquist (FTN) technique can achieve higher spectral and energy efficiencies [3–5]. It, however, requires complicated iterative signal processing algorithms for equalisation at the receiver, which makes the realisation of FTN challenging in practical high-speed systems.

Large signal bandwidth is also necessary for high-capacity wireless systems such as space and terrestrial integrated networks [6, 7], point-to-point wireless backhauls [8], and aerial backbone networks [9]. Millimetre wave (mmWave) frequency bands [10] and even terahertz (THz) frequency bands from 100 GHz to 10 THz [11, 12] have been identified as great options for very high speed communications. Although ISI free transmission at Nyquist rate can be theoretically achieved by conventional Nyquist pulse shaping, signals of large bandwidth require data conversion devices with quite high sampling rate.

However, data conversion devices (e.g. digital-to-analog converter (D/A) and analog-to-digital converter (A/D)) with very high sampling rate are often hard to build and costly. For example, according to the Nyquist sampling theorem, the realisation of single-carrier point-to-point high-speed mmWave communications with signal bandwidth of 10 GHz or wider usually requires 10 giga samples per second (Gsps) or higher D/As and A/Ds, which, however, are difficult to build. One of the most powerful commercial A/Ds released by Analog Device, Inc. (ADI), AD9213, can only achieve 10 Gsps sampling rate with 12 bits resolution [13], while the highest-performance D/A can reach 12.6 Gsps update rate with 16 bits resolution [14]. In addition, the use of a single device with high sampling rate has fairly high requirements on filters, and the transmitted signals usually tend to have slow attenuation, thereby reducing the system spectral efficiency. As a result, advanced signal processing techniques that can enable the use of devices with reduced sampling rates are in high demand.

To solve such technical challenges, channelisation approaches in the time or frequency domain are investigated in, for example [15–18], where the received analog signal is sampled at a fraction of the effective sampling rate in each channel. In [15, 16], time-interleaved D/As or A/Ds based architectures are studied, where multiple parallel low-speed data conversion devices are multiplexed to realise an equivalent high-speed one. However, the differences between multiple practical low-speed data conversion devices degrade the overall performance. From the perspective of implementation, each A/D sees the full bandwidth of input signals, which leads to great difficulty in the sample/hold circuitry design. The required dynamic range of each A/D is also high. Channelising in the frequency domain divides input signals into multiple frequency sub-bands, and an A/D is applied to each sub-band [17, 18]. Although it can greatly ease the requirement on large dynamic range of each A/D, there still exists the same problem in sample/hold circuitry design as in channelising by time-interleaving. Besides, sharp bandpass filters with high centre frequencies for mitigating the effects of strong narrowband interferers are difficult to implement in integrated chips.

By introducing a new concept of complementary Nyquist pulses that satisfy both ISI and cross-symbol interference (CSI) free conditions, a dual pulse shaping (DPS) transmission scheme is proposed to improve spectral efficiency and solve the bottleneck problem of data conversion devices with extremely high sampling rate in [19]. This scheme allows two spectrally overlapped half-symbol-rate channels to be combined without ISI or CSI, achieving full-rate transmission regardless of roll-off factor. Furthermore, symbol-rate based low-complexity linear equalisation methods [20] for DPS transmission are proposed to reduce the required sampling rate of conventional fractionally spaced equalisation [21]. Without requiring any complicated equalisation algorithm, the DPS transmission scheme enables high-speed communications in practical digital hardware.

In this paper, we study single carrier based DPS transmission schemes with ideal sinc-function based complementary Nyquist pulses and their practical approximations, instead of the RC pulses in [22]. In the schemes, the data stream is split into two parallel half-rate data streams with overlapped spectra. This enables full-rate transmission with half-sampling-rate D/As and A/Ds, and meanwhile reduces computational complexity and implementation cost with symbol-rate equalisations. Accordingly, we verify the feasibility of the proposed DPS transmission schemes in a practical high-speed mmWave communication system. Simulation results are provided to compare the proposed DPS transmission schemes with the state of the art [22], in terms of peak-to-average power ratio (PAPR) and bit error rate (BER) performance under typical mmWave fading channels. Butterworth and chebyshev type I low-pass filters (LPFs) with different orders are simulated as the Tx/Rx filters to demonstrate their effects on system performance. Our contributions are summarised as follows:

- Different from the RC based complementary Nyquist pulses used in [19], we consider the use of two new classes of ideal sinc-function based complementary Nyquist pulses for DPS transmission. We demonstrate that the proposed pulses satisfy the ISI-free and CSI-free conditions.
- We propose two sets of practical dual spectral shaping pulses associated with LPFs, each pulse corresponding to different modes of commercial D/As. The one-to-one relationship between the ideal and practical dual shaping pulses is revealed by waveform comparison between the existing and proposed schemes.
- Taking into account the timing offset between dual shaping pulses and carrier-frequency offset (CFO) between transceivers, we carry out performance analysis of both linear zero-forcing (ZF) and minimum mean square error (MMSE) equalisations for DPS transmission. In view of the possible spectral null caused by spectral overlapping in practical symbol interval equalisation, we propose two approaches to improve the robustness of DPS transmission systems by adjusting the clock phase of the D/As and A/Ds. Simulation results show that the spectral null can be effectively suppressed with the adjustment of sampling clock to a proper value.

The remainder of this paper is organised as follows. Section 2 retrospects the Nyquist theorem for ISI-free transmission and introduces DPS transmission with complementary Nyquist pulses under CSI-free criterion. Section 3 proposes two new sets of ideal sinc-function based complementary Nyquist pulses for DPS transmission and demonstrates that they satisfy the ISI-free and CSI-free conditions. Section 4 presents two practical DPS schemes with commercially available D/As and identifies the relationship between the ideal and practical dual shaping pulses. Section 5 analyses the SNR performance after linear equalisation considering the CFO and timing offset between dual shaping pulses, and correspondingly proposes two approaches to avoid the spectral null. In Section 6,

simulation results are provided to demonstrate the performance of the proposed and existing schemes. Finally, the conclusions are provided in Section 7.

The following notations are used throughout this paper. $\mathbf{A}^H$ and $\|\mathbf{A}\|$ denote the conjugate transpose and Frobenius norm of matrix $\mathbf{A}$, respectively; $\mathbf{I}$ is the identity matrix; Further, the notations $\mathbb{E}\{\cdot\}$ and $\mathrm{Tr}\{\cdot\}$ represent the expectation and trace of $\{\cdot\}$, respectively.

2 | DUAL PULSE SHAPING WITH COMPLEMENTARY NYQUIST PULSES

2.1 | Nyquist theorem

In order to avoid ISI, Nyquist pulse shaping is commonly adopted in digital communication systems. Let $h(t)$ represent the overall impulse response of the transmission system to the input symbol. The condition of satisfying ISI free is

$$h(nT_s) = \begin{cases} 1, & n = 0 \\ 0, & n \neq 0 \end{cases} \tag{1}$$

where T_s is the symbol duration. As stated in the Nyquist theorem, the necessary and sufficient condition for (1) is that its Fourier transform $H(f)$ satisfies

$$\sum_{m=-\infty}^{\infty} H\left(f + \frac{m}{T_s}\right) = T_s. \tag{2}$$

Assume the channel bandwidth be W, that is, $H(f) = 0$ for $|f| > W$. There exists only one rectangular window with frequency response $H(f)$ that can lead to (2) when $T_s = \frac{1}{2W}$, that is

$$H_{\Pi}(f) = \begin{cases} T_s, & |f| \leq W \\ 0, & \text{otherwise.} \end{cases} \tag{3}$$

This is equivalently a sinc-function pulse in the time domain given by $\mathrm{sinc}(t/T_s)$, where

$$\mathrm{sinc}(t) = \begin{cases} \sin(\pi t)/\pi t, & t \neq 0 \\ 1, & t = 0. \end{cases} \tag{4}$$

When $T_s > \frac{1}{2W}$, there exist many alternatives for $H(f)$ satisfying (2), and the RC pulse is one of them and has been widely used.

2.2 | Complementary Nyquist pulses

The concept of complementary Nyquist pulses is introduced for DPS transmission in [19]. Consider a half-Nyquist-rate system at a symbol rate of $\frac{1}{2T_s}$. Let $H_N(f)$ represent the spectrum of a Nyquist pulse following $\sum_{m=-\infty}^{\infty} H_N(f + \frac{m}{2T_s}) = 1$. Then the complementary Nyquist pulse spectrum, $H_{CN}(f)$, is defined as

$$H_{CN}(f) = 1 - H_N(f), \quad |f| \leq \frac{1}{2T_s}. \tag{5}$$

This indicates that if the pulses with $H_N(f)$ and $H_{CN}(f)$ are used for two transmitted independent data streams, the full Nyquist rate can be achieved even though they have overlapped spectra. This is referred to as dual pulse shaping transmission. The corresponding classical pair of RC pulse shaping and complementary RC pulse shaping are proposed in [19].

2.3 | Dual pulse shaping transmission under CSI-free criterion

A DPS transmission system can generally transmit two independent data streams using any pair of spectral shaping pulses provided that the pair of spectral shaping pulses meet certain ISI-free and CSI-free conditions.

Denote the pulse shaping spectra of two parallel symbol streams after matched filtering as $|H_1(f)|^2$ and $|H_2(f)|^2$ in a DPS transmission system, both of which satisfy the Nyquist ISI-free condition in (2). As stated in Theorem 1 [22], to prevent the two data streams from mutual interference, a further CSI-free condition also needs to be satisfied

$$\sum_{m=-\infty}^{\infty} H_1\left(f + \frac{m}{2T_s}\right) H_2^*\left(f + \frac{m}{2T_s}\right) = 0. \tag{6}$$

When the Nyquist pulse with the spectrum $H_N(f) = |H_1(f)|^2$ and complementary Nyquist pulse with the spectrum $H_{CN}(f) = |H_2(f)|^2$ are used for the two parallel symbol streams in the DPS transmission system, there exist multiple options for the constructions of these pulses. For example, they can be designed as a root Nyquist pulse and a T_s-delayed root complementary Nyquist pulse that is,

$$\begin{aligned} H_1(f) &= \sqrt{H_N(f)}, \\ H_2(f) &= \sqrt{H_{CN}(f)} e^{-j2\pi f T_s}, \end{aligned} \tag{7}$$

which can be verified to satisfy ISI-free and CSI-free conditions. Alternatively, the two pulses can be designed as

$$\begin{aligned} H_1(f) &= \sqrt{H_N(f)}, \\ H_2(f) &= \begin{cases} -j\sqrt{H_{CN}(f)}, & f \geq 0 \\ j\sqrt{H_{CN}(f)}, & f < 0 \end{cases} \end{aligned} \tag{8}$$

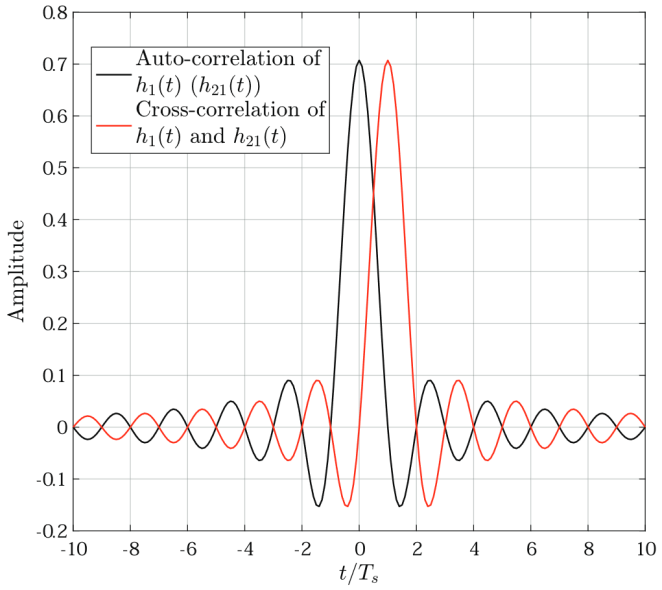

FIGURE 1 The auto-correlation function of $h_1(t)$ ($h_{21}(t)$) and cross-correlation function between $h_1(t)$ and $h_{21}(t)$

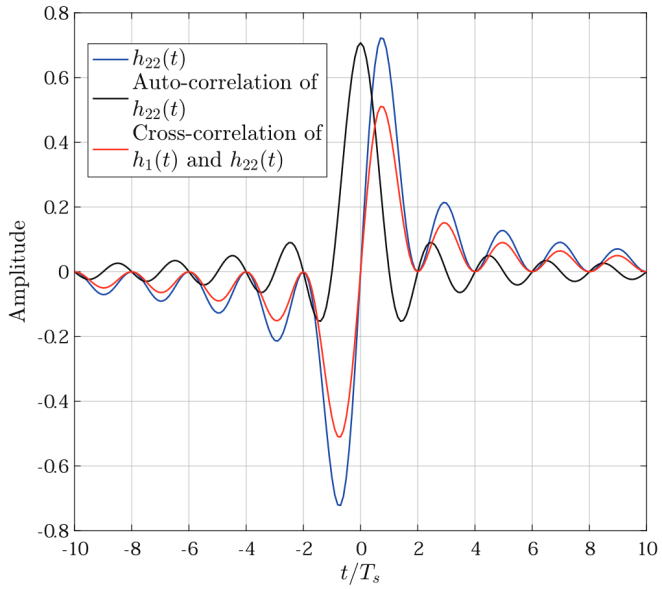

FIGURE 2 $h_{22}(t)$, the auto-correlation function of $h_{22}(t)$ and cross-correlation function between $h_1(t)$ and $h_{22}(t)$

which are a root Nyquist pulse and a Hilbert transformed (or 90° phase shifted version) root complementary Nyquist pulse. They also satisfy ISI-free and CSI-free conditions.[1]

Specifically, when RC and complementary RC spectra are used as $H_N(f)$ and $H_{CN}(f)$ respectively, the corresponding spectra of RRC and root complementary RC (RCRC) are given by

[1] The proposed two sets of pulses in (7) and (8) are only two exemplified designs satisfying ISI-free and CSI-free conditions that we have found so far. They may not be the optimal choices.

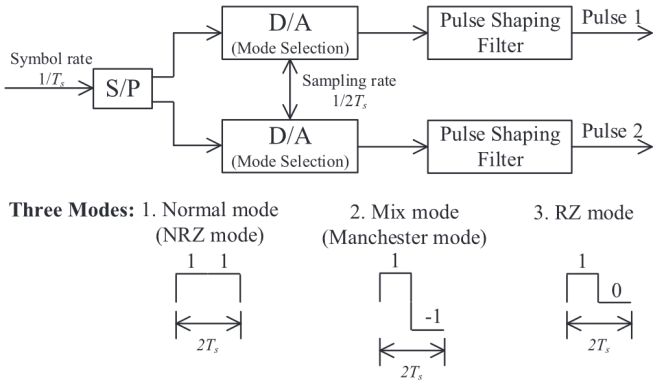

FIGURE 3 DPS transmission block diagram and three D/A operation modes.

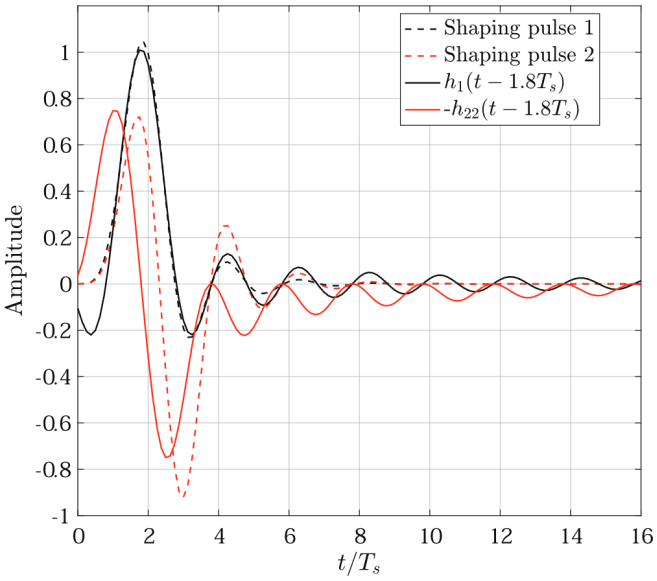

FIGURE 4 Output dual pulses with RZ mode and Manchester mode, compared with $h_1(t-1.8T_s)$ and $-h_{22}(t-1.8T_s)$

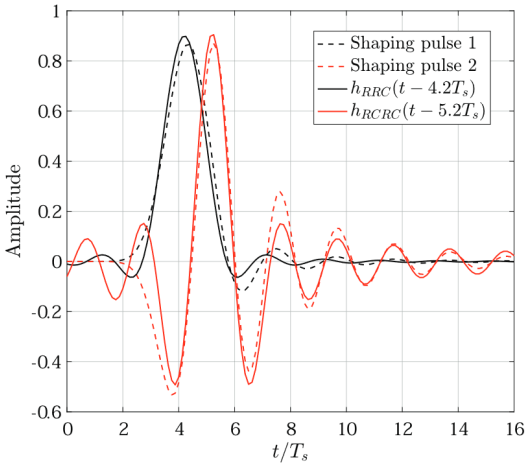

FIGURE 5 Output dual pulses with NRZ mode and Manchester mode with T_s delay, compared with $h_{\mathrm{RRC}}(t-4.2T_s)$ and $h_{\mathrm{RCRC}}(t-5.2T_s)$

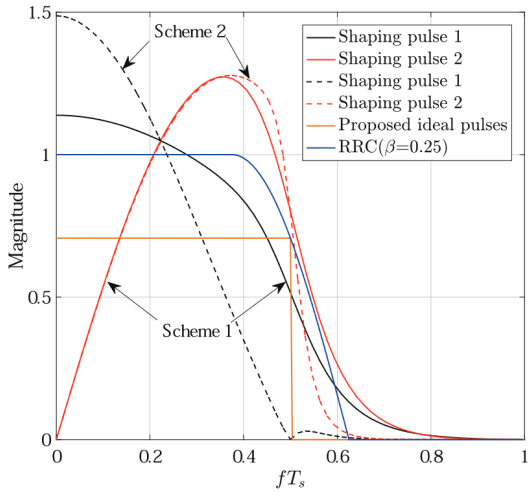

FIGURE 6 Spectra comparison of proposed schemes and RRC

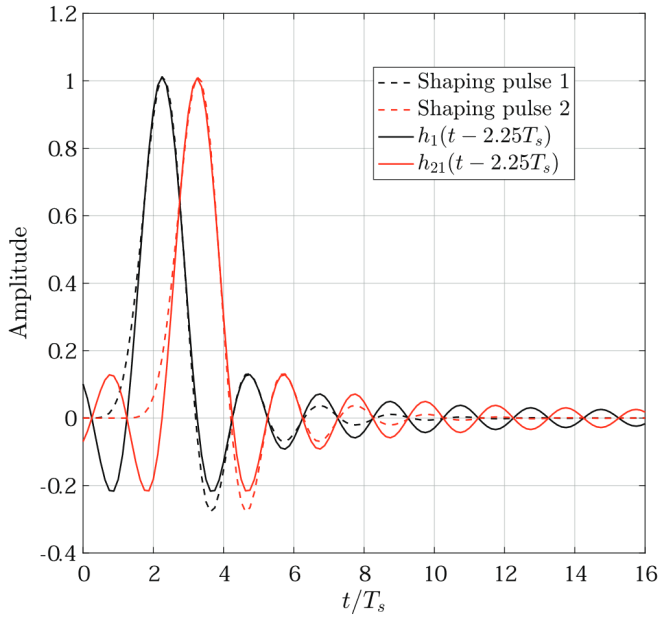

FIGURE 7 Output dual pulses with RZ mode and its T_s delayed version, compared with $h_1(t-2.25T_s)$ and $h_{21}(t-2.25T_s)$

$$H_{\mathrm{RRC}}(f)=\begin{cases}1, & |f|<\dfrac{1-\beta}{4T_s}\\ \cos\left[\dfrac{\pi T_s}{\beta}\left(|f|-\dfrac{1-\beta}{4T_s}\right)\right], & \dfrac{1-\beta}{4T_s}<|f|\le\dfrac{1+\beta}{4T_s}\\ 0, & \text{otherwise}\end{cases} \tag{9}$$

and

$$H_{\mathrm{RCRC}}(f)=\begin{cases}1, & \dfrac{1+\beta}{4T_s}<|f|\le\dfrac{1}{2T_s}\\ \cos\left[\dfrac{\pi T_s}{\beta}\left(|f|-\dfrac{1+\beta}{4T_s}\right)\right], & \dfrac{1-\beta}{4T_s}<|f|\le\dfrac{1+\beta}{4T_s}\\ 0, & \text{otherwise}\end{cases} \tag{10}$$

where β is the roll-off factor taking values in the range $0\le\beta\le 1$. Hence, their corresponding time-domain representations are given by

$$h_{\mathrm{RRC}}(t)=\begin{cases}\dfrac{1-\beta}{2T_s}+\dfrac{2\beta}{\pi T_s}, & t=0\\ \dfrac{\beta}{2\sqrt{2}T_s}\left[\left(1+\dfrac{2}{\pi}\right)\sin\dfrac{\pi}{4\beta}+\left(1-\dfrac{2}{\pi}\right)\cos\dfrac{\pi}{4\beta}\right], & |t|=\dfrac{T_s}{2\beta}\\ \dfrac{\sin\left[\frac{\pi t}{2T_s}(1-\beta)\right]+\frac{2\beta t}{T_s}\cos\left[\frac{\pi t}{2T_s}(1+\beta)\right]}{\pi t\left[1-\left(\frac{2\beta t}{T_s}\right)^2\right]}, & \text{otherwise}\end{cases} \tag{11}$$

and

$$h_{\mathrm{RCRC}}(t)=\begin{cases}\dfrac{1-\beta}{2T_s}+\dfrac{2\beta}{\pi T_s}, & t=0\\ \dfrac{\sin\frac{\pi}{2\beta}}{\pi T_s/2\beta}-\dfrac{\beta}{2\sqrt{2}T_s}\left[\left(1+\dfrac{2}{\pi}\right)\sin\dfrac{\pi}{4\beta}-\left(1-\dfrac{2}{\pi}\right)\cos\dfrac{\pi}{4\beta}\right], & |t|=\dfrac{T_s}{2\beta}\\ \dfrac{\sin\frac{\pi t}{T_s}}{\pi t}-\dfrac{\sin\left[\frac{\pi t}{2T_s}(1+\beta)\right]-\frac{2\beta t}{T_s}\cos\left[\frac{\pi t}{2T_s}(1-\beta)\right]}{\pi t\left[1-\left(\frac{2\beta t}{T_s}\right)^2\right]}, & \text{otherwise.}\end{cases} \tag{12}$$

Also, the odd RCRC (ORCRC) pulses that is, Hilbert transformed pulses, are expressed as

$$h_{\mathrm{ORCRC}}(t)=\begin{cases}0, & t=0\\ -\dfrac{\cos\frac{\pi}{2\beta}}{\pi T_s/2\beta}+\dfrac{\beta}{2\sqrt{2}T_s}\left[\left(1-\dfrac{2}{\pi}\right)\sin\dfrac{\pi}{4\beta}+\left(1+\dfrac{2}{\pi}\right)\cos\dfrac{\pi}{4\beta}\right], & t=\dfrac{T_s}{2\beta}\\ \dfrac{\cos\frac{\pi}{2\beta}}{\pi T_s/2\beta}-\dfrac{\beta}{2\sqrt{2}T_s}\left[\left(1-\dfrac{2}{\pi}\right)\sin\dfrac{\pi}{4\beta}+\left(1+\dfrac{2}{\pi}\right)\cos\dfrac{\pi}{4\beta}\right], & t=-\dfrac{T_s}{2\beta}\\ -\dfrac{\cos\frac{\pi t}{T_s}}{\pi t}+\dfrac{\cos\left[\frac{\pi t}{2T_s}(1+\beta)\right]+\frac{2\beta t}{T_s}\sin\left[\frac{\pi t}{2T_s}(1-\beta)\right]}{\pi t\left[1-\left(\frac{2\beta t}{T_s}\right)^2\right]}, & \text{otherwise.}\end{cases} \tag{13}$$

3 | PROPOSED DUAL PULSE SHAPING WITH SINC-FUNCTION BASED COMPLEMENTARY NYQUIST PULSES

Note that in [19], when the classical pair of RC pulse shaping and complementary RC pulse shaping are designed as Nyquist pulse and complementary Nyquist pulse, they have different time domain waveforms and spectrum properties. In this section, as a supplement to the ideal DPS theory, we propose a pair of identical sinc-function based complementary Nyquist pulses as ideal Nyquist pulse and complementary Nyquist pulse.

The spectra of the proposed sinc-function based complementary Nyquist pulses are given by

$$H_N(f) = H_{CN}(f) = \frac{H_{\Pi}(f)}{2T_s}. \tag{14}$$

By substituting Equation (14) into Equation (7), we have

$$H_1(f) = \begin{cases} 1/\sqrt{2}, & |f| \le \dfrac{1}{2T_s} \\ 0, & \text{otherwise} \end{cases} \tag{15}$$

and

$$H_{21}(f) = \begin{cases} e^{-j2\pi fT_s}/\sqrt{2}, & |f| \le \dfrac{1}{2T_s} \\ 0, & \text{otherwise.} \end{cases} \tag{16}$$

Accordingly, their respective pulses are given by $h_1(t) = \text{sinc}(t/T_s)/\sqrt{2}T_s$ and $h_{21}(t) = h_1(t - T_s)$. The auto-correlation function of $h_1(t)$ ($h_{21}(t)$) and cross-correlation function between $h_1(t)$ and $h_{21}(t)$ can be calculated as $\text{sinc}(t/T_s)/2T_s$ and $\text{sinc}(t/T_s - 1)/2T_s$, respectively, which are shown in Figure 1. It is observed that the value of auto-correlation is zero at $t = \pm 2T_s, \pm 4T_s, ...$, and for cross-correlation at $t = 0, \pm 2T_s, \pm 4T_s, ...$ This observation indicates that the pulses of $h_1(t)$ and $h_{21}(t)$ satisfy the ISI-free and CSI-free conditions.

Substituting (14) into (8), we have

$$H_{22}(f) = \begin{cases} -j/\sqrt{2}, & 0 \le f \le \dfrac{1}{2T_s} \\ j/\sqrt{2}, & -\dfrac{1}{2T_s} \le f < 0. \end{cases} \tag{17}$$

Thus its corresponding Hilbert transformed root complementary Nyquist pulse is given by

$$h_{22}(t) = \begin{cases} \dfrac{1 - \cos\frac{\pi t}{T_s}}{\sqrt{2}\pi t}, & t \ne 0 \\ 0, & t = 0 \end{cases} \tag{18}$$

which is an odd function. Figure 2 shows the waveforms of $h_{22}(t)$, the auto-correlation of $h_{22}(t)$ and cross-correlation between $h_1(t)$ and $h_{22}(t)$, where the functions of auto-correlation and cross-correlation can be computed as $\text{sinc}(t/T_s)/2T_s$ and $h_{22}(t)/\sqrt{2}$, respectively. We can see that the auto-correlation function has zeros periodically spaced in time, and more specifically at time instants $\pm 2T_s, \pm 4T_s, ...$; and for the cross-correlation function, the zeros are at $0, \pm 2T_s, \pm 4T_s, ...$ This means that the pulses of $h_1(t)$ and $h_{22}(t)$ satisfy the ISI-free and CSI-free conditions as well.

Note that with a limited baseband bandwidth of $\frac{1}{2T_s}$, the proposed ideal DPS transmission can jointly achieve the full Nyquist rate of $\frac{1}{T_s}$ with zero ISI and CSI. It can be seen from their mathematical expressions that the proposed sinc-function based complementary Nyquist pulses satisfy the ISI-free and CSI-free conditions, and do not belong to the class of RC and complementary RC Nyquist pulses in [19]. Thus, they can be regarded as a supplement to the theory of DPS transmission. However, the proposed basic pulses are non-causal and impractical, as the sinc-function is infinite and spans over all past and future times. As a result, a pair of delayed and truncated versions are needed to make them realizable that is, one enables $h_1(t - t_0)$, $h_{21}(t - t_0)$ and $h_{22}(t - t_0)$ to approximately equal zero for $t < 0$ by selecting a moderate period of time t_0, and meanwhile shifts the sampling time by t_0. A longer delay generally leads to smaller approximation errors. Furthermore, practical spectral shaping pulses and LPFs, as good approximations to the ideal ones, need to be developed.

4 | SCHEMES FOR PRACTICAL SPECTRAL SHAPING PULSES AND FILTERS

The ideal sinc-function based complementary Nyquist pulses provide an important theoretical basis for DPS transmission. In the following, we propose two schemes for practical spectral shaping pulses and filters, and show the one-to-one relationship between ideal and practical dual spectral shaping pulses by comparing with the existing schemes.

As described in the data-sheet of commercial D/As [23], the D/A core is enabled to operate in one of the following three modes: normal mode (nonreturn-to-zero (NRZ) mode), mix mode (Manchester mode), and return-to-zero (RZ) mode, which can be selected via serial port interface register. In fact, any mode with a practical shaping filter can be used to generate a spectral shaping pulse, from which DPS transmission is formed as shown in the block diagram of Figure 3. The data symbol stream at a symbol rate of $\frac{1}{T_s}$ is split into two half-rate parallel streams by a serial-to-parallel converter (S/P). Then, they are converted into analog signals via the D/As at the sampling rate of $\frac{1}{2T_s}$, where the corresponding mode is selected in D/As. After the analog signals pass through the pulse shaping filters, the desirable shaping pulses are formed to generate the baseband signals by a transmitting filter.

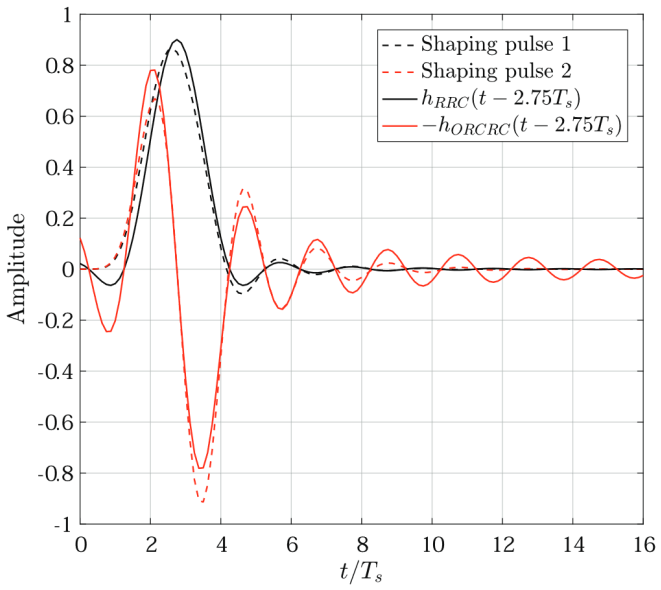

FIGURE 8 Output dual pulses with NRZ mode and Manchester mode, compared with $h_{\mathrm{RRC}}(t-2.75T_s)$ and $-h_{\mathrm{ORCRC}}(t-2.75T_s)$

We propose the first scheme where an RZ pulse and a Manchester pulse are used for DPS transmission. After transmit pulse shaping with a sixth order butterworth LPF, the two spectral shaping pulses are shown in Figure 4, where the proposed $h_1(t)$ and $-h_{22}(t)$ given by Equation (17) with an appropriate time delay are also plotted for comparison. An appropriate time delay is introduced to make the proposed ideal dual pulse shaping realizable. Note that, to show similar time domain waveforms of shaping pulses between the proposed schemes and the corresponding ideal ones, we intentionally add time delays of $1.8T_s$, $4.2T_s$, and $2.25T_s$ for ideal ones in Figures 4, 5, and 7, respectively, to test the case when the main lobes of two shaping pulses are overlapped. We propose the second scheme using an NRZ pulse and a T_s-delayed Manchester pulse. The spectral shaping pulses after a 16th order butterworth LPF are shown in Figure 5. As a comparison, the waveforms of the delayed $h_{\mathrm{RRC}}(t)$ and $h_{\mathrm{RCRC}}(t-T_s)$ given by (10) and (11) are displayed with a roll-off factor $\beta=1$. It is observed that the proposed schemes have similar time domain waveforms of shaping pulses to the corresponding ideal ones. Their frequency responses are also shown in Figure 6. It can be seen that the dual shaping pulses of each DPS scheme occupy the same signal spectrum, and the ones with higher order filters have a shorter transition region. The spectra of the proposed ideal pulses and conventional Nyquist RRC pulses with $\beta=0.25$ are also plotted for comparison.

Also, two sets of practical dual spectral shaping pulses presented in the two schemes in [22] are shown in Figures 7 and 8, respectively. For convenience, we call them scheme 3 and scheme 4 in this paper. Here, scheme 3 employs an RZ pulse and its T_s delayed version, and scheme 4 adopts an NRZ pulse and a Manchester pulse. It can be seen that the former, after passing an eighth order butterworth LPF, matches the proposed sinc-function based dual shaping pulses very well. The latter, after passing the same filter, provides very similar dual shaping pulses to the delayed ideal $h_{\mathrm{RRC}}(t)$ and $-h_{\mathrm{ORCRC}}(t)$ given by Equation (12) with $\beta=1$.

TABLE 1 Relationship between practical and ideal dual shaping pulses

Scheme	Practical pulses (Mode)	Ideal pulses
1	RZ mode and Manchester mode	$h_1(t)$ and $h_{22}(t)$
2	NRZ mode and Manchester mode with T_s delay	$h_{\mathrm{RRC}}(t)$ and $h_{\mathrm{RCRC}}(t-T_s)$
3	RZ mode and RZ mode with T_s delay	$h_1(t)$ and $h_1(t-T_s)$
4	NRZ mode and Manchester mode	$h_{\mathrm{RRC}}(t)$ and $h_{\mathrm{ORCRC}}(t)$

The one-to-one relationship between practical and ideal dual shaping pulses is summarised in Table 1. It indicates that the schemes of practical DPS, as approximations of the ideal DPS with an appropriate time delay, can be implemented by mode selection in attainable D/As. Although the butterworth filter is used in the above schemes due to its maximally flat frequency response in the passband, other types of LPFs (e.g. chebyshev filters) can also be used for DPS. Furthermore, the LPF design, for example, the selection of the filter order, plays a significant role in generating the desired pulse shaping. In real DPS transmission systems, suitable filter types and design parameters can be selected according to specific performance requirements. As the transition from pass-band to stop-band is necessary for any practical pulse, effective and implementable equalisation is commonly needed to remove both ISI and CSI.

5 | PERFORMANCE OF LINEAR EQUALISATION CONSIDERING TIMING OFFSET BETWEEN DUAL SHAPING PULSES AND CARRIER FREQUENCY OFFSET

Since various distortions exist in wireless transmission channels, equalisation at the receiver is required to cancel both ISI and CSI. The symbol interval equalisation with the symbol-rate sampling usually causes spectral overlapping at the two edges of the signal spectrum, and even the spectral null may occur, which leads to degraded equalisation performance. In this section, we analyse the SNR performance after linear equalisation considering the timing offset between dual shaping pulses and CFO, and then propose two approaches to improve the robustness of DPS by adjusting the clock phase of the D/As or A/Ds.

5.1 | Transmitter and receiver

The block diagrams of the DPS transmitter and receiver are shown in Figure 9, where the radio frequency chains

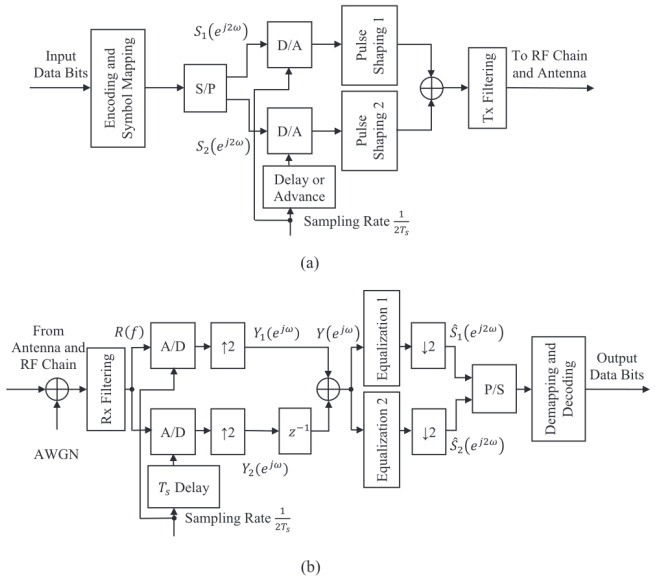

FIGURE 9 (a) DPS transmitter with the timing offset between dual shaping pulses and (b) receiver

(e.g. the up/down converters, high power amplifier, and low noise amplifier) and Tx/Rx antennas are not shown for simplicity.

The transmitter firstly encodes the input data bits and maps them into data symbols followed by an S/P conversion. With half-symbol-rate sampling, the two parallel data symbol streams are converted into analog signals by the D/As, and then combined after passing through their respective pulse shaping filters. Note that the clock phase of the second D/A can be adjusted to delay or advance the impulse response of the pulse shaping filter. The transmitted baseband signals are formed by filtering the combined signal with a Tx filter. The receiver firstly filters the received baseband signal with a Rx filter, followed by two separate A/Ds at a sampling rate equal to half of the symbol rate. The two generated digital signal streams are up-sampled by a ratio of two, and then combined after the second data stream being delayed by one sample. Note that the A/D samples the second data stream with a T_s delay. The combined digital signal stream is equalised by two equalisers, and then down-sampled by a ratio of two, respectively, to obtain two recovered transmitted data symbols streams. The two parallel streams are converted into one serial stream by a parallel-to-serial (P/S) conversion. Finally, the original data bits are retrieved by demapping and decoding.

5.2 | Signal models

Let $S_1(e^{j2\omega})$ and $S_2(e^{j2\omega})$ represent the Fourier transforms of the two parallel sequences after S/P conversion. Let $H_1(f)$ and $H_2(f)$ represent the frequency responses for the equivalent DPS channels including their respective pulse shaping filters, Tx/Rx filters and physical channels, and $W(f)$ denote the additive white Gaussian noise (AWGN) in the frequency domain at the receiver. Note that ω and f are the digital frequency and analog frequency respectively with $\omega = 2\pi f T_s$. Considering the timing offset between dual shaping pulses and CFO between the transmitter and receiver, the received signal after the Rx filter in the frequency domain is given by

$$\begin{aligned} R(f) =& H_1(f-\Delta f)S_1(e^{j4\pi(f-\Delta f)T_s}) \\ &+ H_2(f-\Delta f)S_2(e^{j4\pi(f-\Delta f)T_s})e^{-j2\pi(f-\Delta f)T_s\tau} \\ &+ W(f), \end{aligned} \tag{19}$$

where Δf denotes the CFO introduced at the receiver, and τ denotes the normalised delay (positive value) or advance (negative value) between two transmission pulses (normalised by T_s).

After $R(f)$ is sampled by two A/Ds with sampling rate $\frac{1}{2T_s}$ and then up-sampled by two, respectively, two output digital signals in the frequency domain can be given by

$$\begin{aligned} Y_1(e^{j\omega}) =& \frac{S_1(e^{j2\omega'})}{2T_s}\sum_{k=-\infty}^{+\infty} H_1\left(\frac{\omega'}{2\pi T_s}-\frac{k}{2T_s}\right) \\ &+ \frac{S_2(e^{j2\omega'})}{2T_s}\sum_{k=-\infty}^{+\infty} e^{j(\pi k-\omega')\tau}H_2\left(\frac{\omega'}{2\pi T_s}-\frac{k}{2T_s}\right) \\ &+ \frac{1}{2T_s}\sum_{k=-\infty}^{+\infty} W\left(\frac{\omega}{2\pi T_s}-\frac{k}{2T_s}\right) \end{aligned} \tag{20}$$

and

$$\begin{aligned} &Y_2(e^{j\omega}) \\ &= \frac{e^{j\omega'}}{2T_s}S_1(e^{j2\omega'})\sum_{k=-\infty}^{+\infty}(-1)^k H_1\left(\frac{\omega'}{2\pi T_s}-\frac{k}{2T_s}\right) \\ &\quad+ \frac{e^{j\omega'}}{2T_s}S_2(e^{j2\omega'})\sum_{k=-\infty}^{+\infty}(-1)^k e^{j(\pi k-\omega')\tau}H_2\left(\frac{\omega'}{2\pi T_s}-\frac{k}{2T_s}\right) \\ &\quad+ \frac{e^{j\omega'}}{2T_s}\sum_{k=-\infty}^{+\infty}(-1)^k W\left(\frac{\omega}{2\pi T_s}-\frac{k}{2T_s}\right), \end{aligned} \tag{21}$$

respectively, where $\omega' = \omega - \Delta\omega$ and $\Delta\omega = 2\pi\Delta f T_s$.

After $Y_2(e^{j\omega})$ is delayed one sample and then added to $Y_1(e^{j\omega})$, we have the combined signal $Y(e^{j\omega}) = Y_1(e^{j\omega}) + e^{-j\omega'}Y_2(e^{j\omega})$. Let $\mathbf{Y}(\omega,\tau) = [Y(e^{j\omega}), Y(e^{j(\omega-\pi)})]^T$, and see the Appendix for its derivation. After applying the digital equalisation,

$$\mathbf{C}(\omega',\tau) = \begin{bmatrix} C_1(e^{j\omega'})C_1(e^{j(\omega'-\pi)}) \\ C_2(e^{j\omega'})C_2(e^{j(\omega'-\pi)}) \end{bmatrix}$$

to $\mathbf{Y}(\omega,\tau)$ and then down-sampling the equalised signals by two, we obtain the estimates of $S_1(e^{j2\omega})$ and $S_2(e^{j2\omega})$ as

$$\hat{\mathbf{S}}(\omega)=\begin{bmatrix}\hat{S}_1(e^{j2\omega})\\ \hat{S}_2(e^{j2\omega})\end{bmatrix}=\mathbf{C}(\omega',\tau)\mathbf{Y}(\omega,\tau), \tag{22}$$

where the low-complexity linear equalisers can be derived as will be detailed in next subsection.

5.3 | Linear equalisation

5.3.1 | ZF equalisation

Assuming that the channel matrix is perfectly known at the receiver, the ZF equalisation matrix $\mathbf{C}(\omega',\tau)$ can be obtained by calculating its inverse that is, $\mathbf{C}(\omega',\tau)=\mathbf{H}^{-1}(\omega',\tau)$. Substituting (35) into (23), the received signal after ZF equalisation is given by

$$\hat{\mathbf{S}}(\omega)=\mathbf{S}(\omega')+\mathbf{H}^{-1}(\omega',\tau)\mathbf{W}(\omega). \tag{23}$$

Assuming the noise with power spectral density σ^2, the noise power spectral density after ZF equalisation is

$$\mathbb{E}\left\{\left\|\mathbf{H}^{-1}(\omega',\tau)\mathbf{W}(\omega)\right\|^2\right\}=\sigma^2\left\|\mathbf{H}^{-1}(\omega',\tau)\right\|^2. \tag{24}$$

Assuming that the transmitted signals are independent with power spectral density s^2, the output SNR after ZF equalisation is given by

$$\gamma_{\mathrm{ZF}}=\frac{\int_0^{\pi}2s^2d\omega}{\int_0^{\pi}\sigma^2\left\|\mathbf{H}^{-1}(\omega',\tau)\right\|^2d\omega}=\frac{2\pi\rho}{\int_0^{\pi}\left\|\mathbf{H}^{-1}(\omega',\tau)\right\|^2d\omega}, \tag{25}$$

where $\rho=s^2/\sigma^2$ is the average SNR at the input of the receiver with the power of the channel impulse response normalised to 1.

Therefore, the SNR degradation after ZF equalisation, with respect to the input SNR at the receiver, can be calculated as

$$D_{\mathrm{ZF}}=\frac{\int_0^{\pi}\left\|\mathbf{H}(\omega',\tau)\right\|^2d\omega\int_0^{\pi}\left\|\mathbf{H}^{-1}(\omega',\tau)\right\|^2d\omega}{4\pi^2}. \tag{26}$$

To evaluate the effect of the timing offset between dual shaping pulses on the output SNR performance, we define the ratio of the output SNR with timing offset to that without timing offset as the SNR gain, G_{ZF}, and it is calculated as

$$G_{\mathrm{ZF}}=\frac{\int_0^{\pi}\left\|\mathbf{H}^{-1}(\omega',0)\right\|^2d\omega}{\int_0^{\pi}\left\|\mathbf{H}^{-1}(\omega',\tau)\right\|^2d\omega}. \tag{27}$$

5.3.2 | MMSE equalisation

The MMSE equalisation matrix $\mathbf{C}(\omega',\tau)$ can be given by

$$\mathbf{C}(\omega',\tau)=\mathbf{H}^H(\omega',\tau)\left(\mathbf{H}(\omega',\tau)\mathbf{H}^H(\omega',\tau)+\mathbf{I}/\rho\right)^{-1}, \tag{28}$$

and its corresponding MMSE is derived by

$$\begin{aligned}&\mathbb{E}\left\{\left\|\mathbf{C}(\omega',\tau)\mathbf{Y}(\omega,\tau)-\mathbf{S}(\omega')\right\|^2\right\}\\&=\mathrm{Tr}\left\{\mathbb{E}\left\{\left(\mathbf{C}(\omega',\tau)\mathbf{Y}(\omega,\tau)-\mathbf{S}(\omega')\right)\mathbf{Y}^H(\omega,\tau)\mathbf{C}^H(\omega',\tau)\right\}\right\}\\&+\mathrm{Tr}\left\{\mathbb{E}\left\{\left(\mathbf{S}(\omega')-\mathbf{C}(\omega',\tau)\mathbf{Y}(\omega,\tau)\right)\mathbf{S}^H(\omega')\right\}\right\}\\&\overset{(a)}{=}\mathrm{Tr}\left\{\mathbb{E}\left\{\left(\mathbf{S}(\omega')-\mathbf{C}(\omega',\tau)\mathbf{Y}(\omega,\tau)\right)\mathbf{S}^H(\omega')\right\}\right\}\\&=s^2\mathrm{Tr}\left\{\mathbf{I}-\mathbf{C}(\omega',\tau)\mathbf{H}(\omega',\tau)\right\},\end{aligned} \tag{29}$$

where (a) holds in terms of the orthogonality principle that is, $\mathbb{E}\{(\mathbf{C}(\omega',\tau)\mathbf{Y}(\omega,\tau)-\mathbf{S}(\omega'))\mathbf{Y}^H(\omega,\tau)\}=0$. Therefore, the SNR after MMSE equalisation is

$$\begin{aligned}\gamma_{\mathrm{MMSE}}&=\frac{\int_0^{\pi}s^2\left(2-\mathrm{Tr}\left\{\mathbf{I}-\mathbf{C}(\omega',\tau)\mathbf{H}(\omega',\tau)\right\}\right)d\omega}{\int_0^{\pi}s^2\mathrm{Tr}\left\{\mathbf{I}-\mathbf{C}(\omega',\tau)\mathbf{H}(\omega',\tau)\right\}d\omega}\\&=\frac{\int_0^{\pi}\mathrm{Tr}\left\{\mathbf{C}(\omega',\tau)\mathbf{H}(\omega',\tau)\right\}d\omega}{2\pi-\int_0^{\pi}\mathrm{Tr}\left\{\mathbf{C}(\omega',\tau)\mathbf{H}(\omega',\tau)\right\}d\omega}.\end{aligned} \tag{30}$$

Likewise, the SNR degradation after MMSE equalisation is

$$\begin{aligned}D_{\mathrm{MMSE}}=&\rho\int_0^{\pi}\left\|\mathbf{H}(\omega',\tau)\right\|^2d\omega\\&\times\left(\frac{1}{\int_0^{\pi}\mathrm{Tr}\left\{\mathbf{C}(\omega',\tau)\mathbf{H}(\omega',\tau)\right\}d\omega}-\frac{1}{2\pi}\right).\end{aligned} \tag{31}$$

The corresponding SNR gain, G_{MMSE}, is calculated as

$$\begin{aligned}G_{\mathrm{MMSE}}=&\frac{\int_0^{\pi}\mathrm{Tr}\left\{\mathbf{C}(\omega',\tau)\mathbf{H}(\omega',\tau)\right\}d\omega}{\int_0^{\pi}\mathrm{Tr}\left\{\mathbf{C}(\omega',0)\mathbf{H}(\omega',0)\right\}d\omega}\\&\times\frac{2\pi-\int_0^{\pi}\mathrm{Tr}\left\{\mathbf{C}(\omega',0)\mathbf{H}(\omega',0)\right\}d\omega}{2\pi-\int_0^{\pi}\mathrm{Tr}\left\{\mathbf{C}(\omega',\tau)\mathbf{H}(\omega',\tau)\right\}d\omega}.\end{aligned} \tag{32}$$

5.4 | Avoiding spectral null in equalisation of DPS transmission systems

A spectral null may be introduced within the overlapped spectrum resulting from the symbol-rate sampling. For example, if the channel introduces 90° phase shift to the transmitted

signal, that is $H(f) = \begin{cases} j, & f \geq 0 \\ -j, & f < 0 \end{cases}$, a spectral null will appear at the edge of the signal spectrum after A/D, which significantly degrades the equalisation performance. To this end, we present two approaches to avoid the spectral null for the DPS transmission system by adjusting the second D/A and A/D clock phases, respectively, and hence the delay or advance of the spectral shaping pulses. As shown in Figure 9a that delay or advance is added to the second D/A at the transmitter, the proposed approach I involves the following steps:

1) Set the clock phase of the second D/A to an initial value.
2) Transmit a test signal through the channel and loop back the test signal to the receiver.
3) Estimate the channel frequency responses and further the SNR of the equalised data symbols.
4) Adjust the clock phase of the second D/A to obtain a delayed or advanced spectral shaping pulse.
5) Repeat steps (2) to (4) and determine the optimal clock phase with the highest SNR.

Note that the above steps describe an offline static calibration of the transmitter. Instead, an online adaptive calibration can also be achieved by transmitting the testing signal to a remote receiver at step (2), and feeding back the SNR through a return link to the transmitter at step (3).

Similarly, delay or advance can also be added to the second A/D at the receiver. The proposed approach II includes the following steps:

1) Set the clock phase of the second A/D to an initial value.
2) Transmit a test signal at the transmitter.
3) Estimate the channel frequency responses and further the SNR of the equalised data symbols.
4) Adjust the clock phase of the second A/D to obtain a delayed or advanced sampling signal.
5) Repeat steps (2) to (4) and determine the optimal clock phase with the highest SNR.

5.5 | Performance evaluation of the proposed approaches

To evaluate the robustness of the proposed approaches, we compare the equalisation performance for systems with different relative sampling delays for the second D/A or A/D between the DPS and conventional SPS transmissions, when there exists spectral null in channel frequency response. Here, we take the RRC pulse and its T_s-delayed version as the example, and set the SNR ρ to 27 dB.

Firstly, we assume the CFO to be zero, the SNR degradation after equalising the signals passing through a channel with 90° phase shift is plotted in Figure 10, where the normalised delay τ of the second D/A or A/D varies from -1 to 1 and a roll-off factor $\beta = 0.25$ is used. It is seen from Figure 10

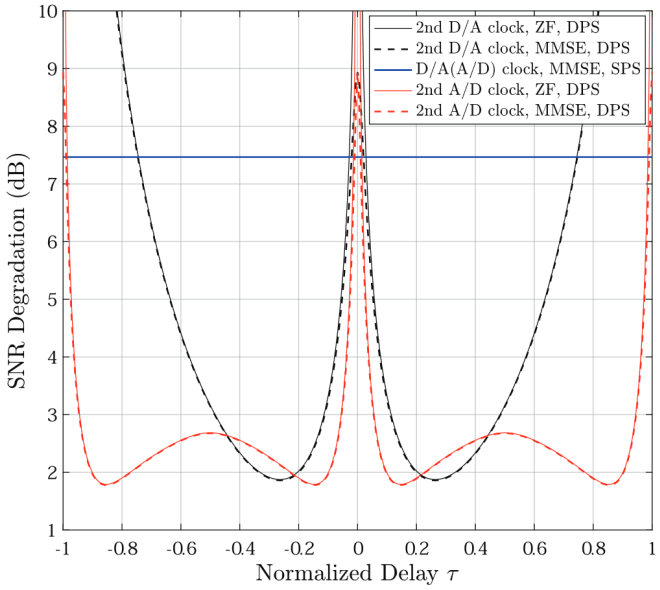

FIGURE 10 Comparison of SNR degradation after equalisation between the DPS and conventional SPS transmissions versus the normalised delay

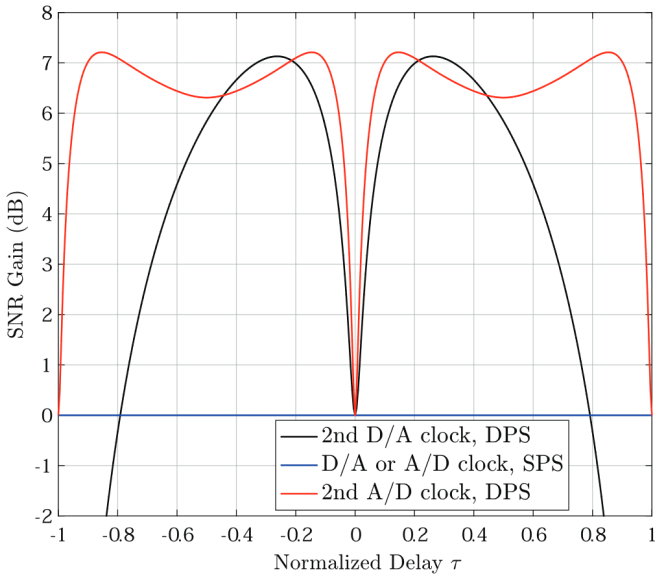

FIGURE 11 The SNR gain with timing offset relative to that without timing offset

that without clock phase change, the conventional SPS transmission outperforms the DPS transmission by about 1.5 dB for MMSE equalisation. However, with clock phase adjustment, the DPS transmission surpasses the SPS transmission by up to 5.6 dB for the second D/A at $\tau = \pm 0.27$ and 5.7 dB for the second A/D at $\tau = \pm 0.15$ and ± 0.85, respectively. Note that with digitally controlled phase shifters, a fractional delay can be easily implemented by changing the clock phase of D/A or A/D.

Figure 11 shows the SNR gain with timing offset relative to that without timing offset employing MMSE equalisation. We can see that similarly to Figure 10, the highest gain of

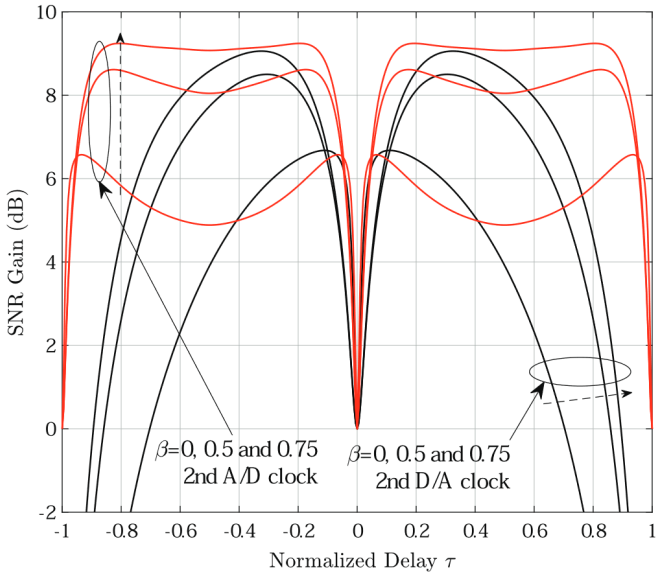

FIGURE 12 The SNR gain using the RRC filter with the roll-off factor β = 0, 0.5, and 0.75

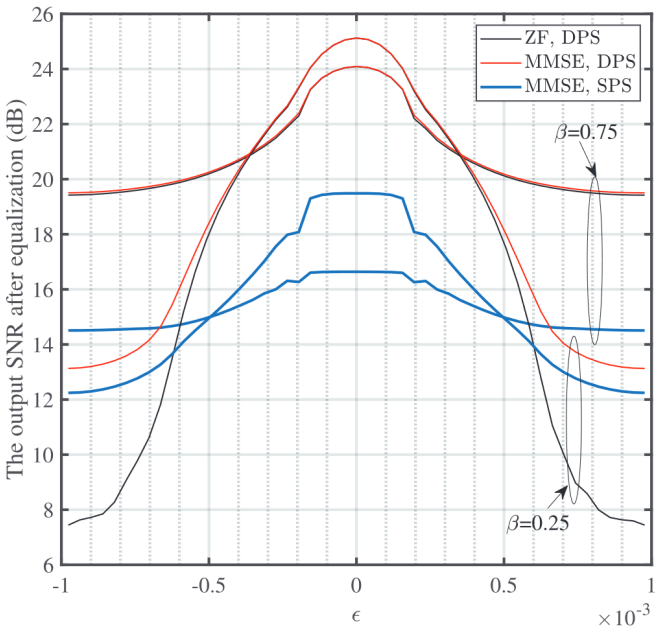

FIGURE 13 The output SNR after equalisation versus the normalised CFO ε

7.13 dB appears at $\tau = \pm 0.27$ by adjusting the second D/A, while 7.21 dB at $\tau = \pm 0.15$ and ± 0.85 for the second A/D. It indicates that the optimal clock phases (i.e. the timing offsets) can be determined by the proposed approaches to achieve the best equalisation performance.

Figure 12 shows the SNR gain using the RRC filter with the roll-off factor $\beta = 0$, 0.5, and 0.75, where the dashed arrows point out the value order of roll-off factors. It is observed that the SNR gain can be maximised for any given roll-off factor by adjusting the second D/A or A/D clock phase to an appropriate value. The maximised gain is roll-off factor dependent. When $\beta = 0$, the maximised gains are only 6.68 dB at $\tau = \pm 0.11$ for the second D/A, and 6.57 dB at $\tau = \pm 0.07$ and $\tau = \pm 0.93$ for the second A/D, respectively. The maximised gain increases with the increase of β.

Figure 13 shows the output SNR after equalisation versus the normalised CFO ε using the RRC filter with β=0.25 and 0.75, where ε is defined as the CFO normalised to $1/T_s$ and varies from -10^{-3} to 10^{-3}. It can be seen from the figure that the output SNR performance after equalisation degrades with the increase of ε. Both ZF and MMSE equalisations using DPS exhibit almost the same performance with β=0.75, which is better than that of SPS, where τ is set to the optimal value of 0.27 by adjusting clock phase of the second D/A of DPS. For β=0.25, MMSE outperforms ZF as ε increases, whereas the drop rates of both steeply exceed those with β=0.75, although they have higher output SNRs in the ideal case without CFO (i.e. ε=0).

6 | SIMULATION RESULTS

In this section, we present the simulation results for DPS transmission systems using the proposed schemes, as well as existing schemes for comparison.

6.1 | System configuration

To evaluate the feasibility of DPS schemes for high-speed wireless applications, we consider an mmWave communication system operating at the 71–76 GHz E-band. With the 5 GHz bandwidth, the 64-QAM is used to realise 6 bps/Hz spectral efficiency, and hence achieving 30 Gbps data rate including some signalling overhead. Instead of 5 Gsps D/As and A/Ds, low-cost ones with sampling rate of 2.5 Gsps are applied at the transceiver. Linear ZF equaliser is employed in simulations to provide the BER performance. Also, both butterworth and chebyshev type I LPFs with different parameter settings are simulated to investigate their effects on system performance. In simulation, we consider mmWave channel models [24] in point-to-point transmission environments characterised by the dominant line-of-sight (LOS) component and non-LOS (NLOS) scattering components, where the power ratio of the LOS path to NLOS path, η, and NLOS path time delay relative to LOS path, T_d, are set to 3 dB and 6 ns, respectively.

6.2 | Performance comparison

The PAPR performance of our proposed DPS schemes is compared with the existing ones in Figure 14. The x-axis, $PAPR_0$, denotes the predefined thresholds of PAPR, while the y-axis denotes the probability of PAPR larger than $PAPR_0$. For a fair comparison, the same LPFs are used for DPS schemes. It is seen that scheme 2 achieves almost the same PAPR performance as scheme 4. Scheme 1 exhibits worse performance than the others even though it is slightly better when $PAPR_0$ is low. Scheme 3 provides the best PAPR performance among all DPS schemes,

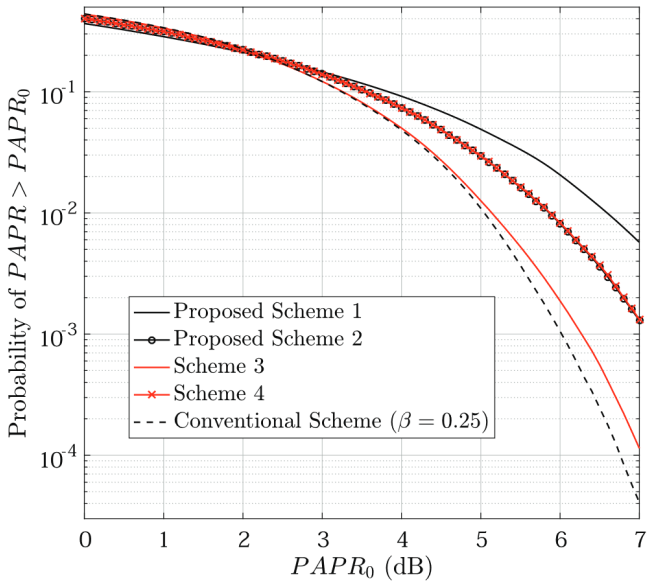

FIGURE 14 PAPR comparison between different schemes

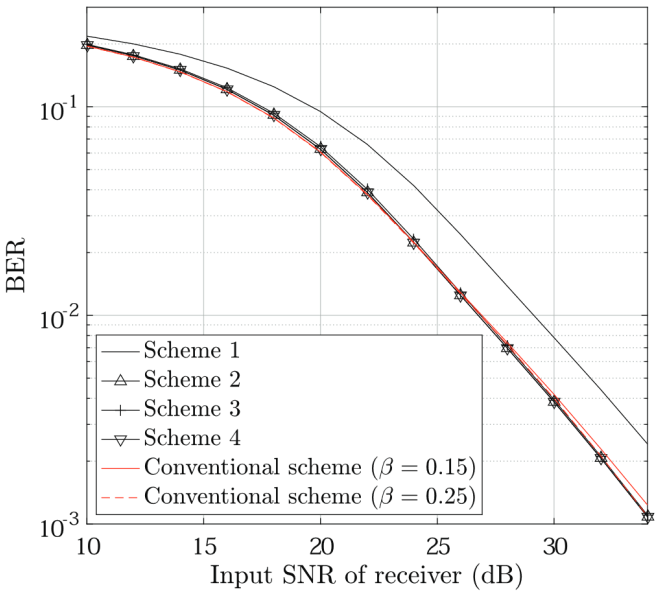

FIGURE 16 BER comparison between different schemes

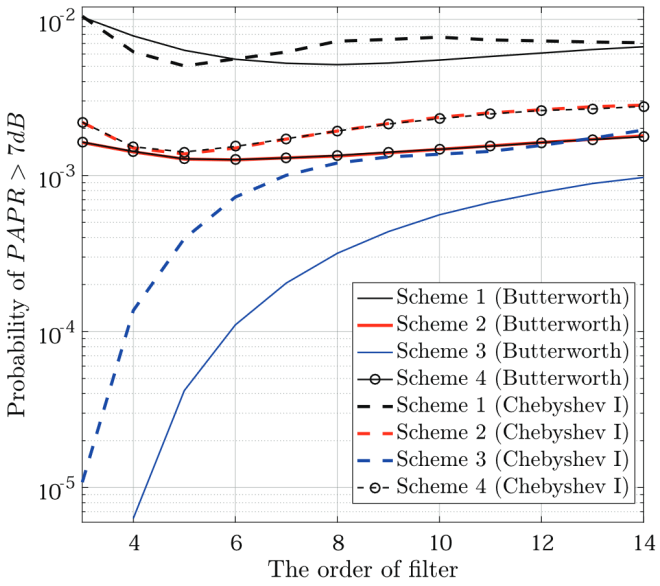

FIGURE 15 PAPR versus the order of LPF

which approaches that of the conventional scheme with a roll-off factor $\beta = 0.25$. Although the conventional one with single RRC pulse shaping achieves improved PAPR performance with the increasing $PAPR_0$, it requires D/As with a doubled sampling rate compared to DPS schemes.

Figure 15 compares the PAPR performance versus the order of LPF between the proposed and existing DPS schemes, where the peak-to-peak passband ripple of the chebyshev LPF is fixed to 0.5 dB. For scheme 1 with the butterworth LPF, the optimal PAPR performance appears at order eight, whereas with chebyshev LPF, order five achieves the optimal PAPR performance. Scheme 2 has very close performance to scheme 4, while scheme 3 has the lowest probability of PAPR over 7 dB, which are consistent with those for Figure 14. The PAPR performance generally improves with the decreasing order of LPF. Particularly, scheme 3 is most sensitive to the order of LPF. Butterworth LPF is superior to chebyshev LPF in terms of the PAPR performance, since the former without ripple rolls off more slowly around the cutoff frequency than the latter.

Without considering any practical impairment, we compare the (uncoded) BER performance of DPS schemes. Figure 16 presents the BER performance as a function of the input SNR at the receiver ranging from 10 to 34 dB, where the sixth order butterworth LPFs are used. For comparison, the BERs of conventional schemes under $\beta = 0.15$ and 0.25 are also plotted. It is shown that, the curves of schemes 2 and 4 are overlapped, and both schemes achieve slightly lower BER than schemes 3. Also, their BER performance is close to that of the conventional scheme with $\beta = 0.25$, and slightly better than that with $\beta = 0.15$ when the SNR is high. Scheme 1 has higher BER than the others, since the difference between practical and ideal dual shaping pulses for scheme 1, as shown in Figure 4, is larger than those of other schemes.

Figure 17 shows the BER of DPS schemes versus the order of LPF using different types of LPFs, where the SNR is fixed to 30 dB. As shown in the figure, the BER for using butterworth LPFs fluctuates with the variation of the order of LPF, whereas for chebyshev type I LPFs it is relatively more stable when the order is above five. For butterworth LPFs, the even numbered orders exhibit lower BERs than the odd numbered ones. Also, butterworth LPFs show lower BERs than chebyshev type I LPFs when the order is even. The variation in order causes the changes of overall channel frequency responses including Tx/Rx filters, thus the output SNR after ZF equalisation. Schemes 2 and 4 have nearly the same BER and slightly outperform scheme 3, which consist with the corresponding results in Figure 16.

Figure 18 shows the wireless propagation channel effect on the BER of DPS schemes, where only the curves of scheme

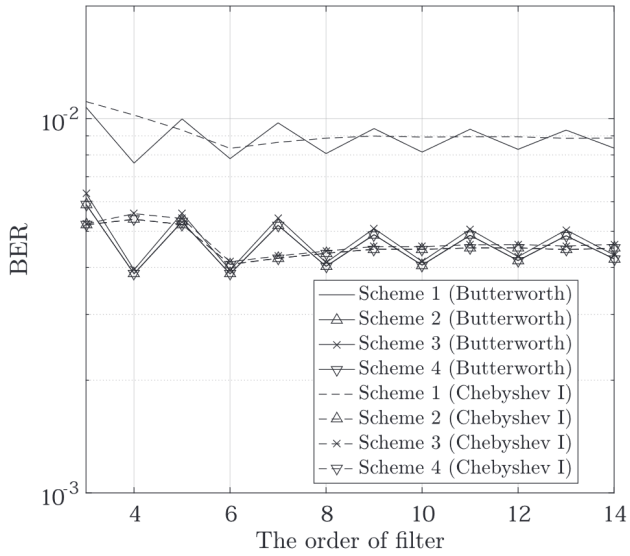

FIGURE 17 BER versus the order of LPF

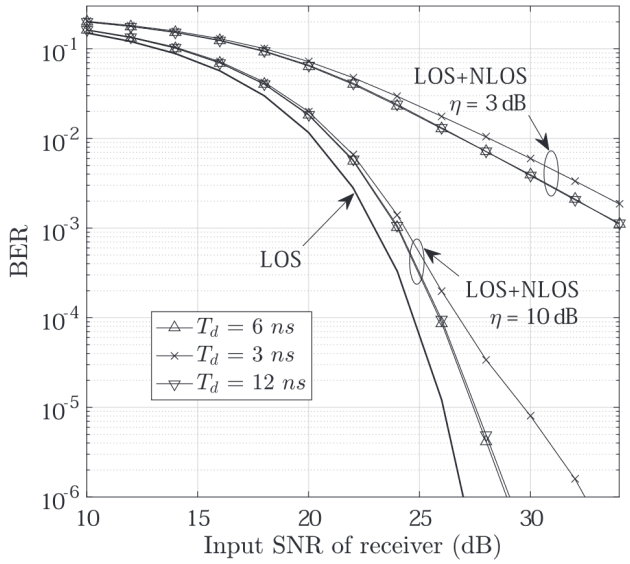

FIGURE 18 The wireless propagation channel effect on BER performance

3 are displayed for the clarity of illustration. It is seen from Figure 18 that the BER is notably increased from the case with a single LOS path to that with LOS plus NLOS paths. When the power ratio of LOS path to NLOS paths, η, is 3 dB, DPS schemes have over 11 dB SNR loss at the BER of 10^{-3}. From the figure, we can see a significant improvement, as much as 10 dB, when η reaches 10 dB. As the NLOS path time delay, T_d, decreases from 6 to 3 ns, the BER performance degrades, whereas it is close to that when T_d increases to 12 ns.

7 | CONCLUSION

We have studied DPS transmission with two classes of ideal sinc-function-based complementary Nyquist pulses, which enables full Nyquist rate using D/As with the sampling rate equal to only half of the data symbol rate. The ISI-free and CSI-free conditions are theoretically verified for the proposed dual shaping pulses. We propose two sets of practical dual spectral shaping pulses based on commercially available D/As. Through illustration and comparison between the existing and proposed schemes, we disclose the relationship between ideal and practical dual shaping pulses. We analyse the equalisation performance when the timing offset exists between dual shaping pulses. We also proposed approaches to avoid spectral null, which can practically improve the robustness of DPS transmission, by adjusting the clock phase of the D/As or A/Ds. Simulation results show that an RZ pulse and its T_s delayed version is an excellent choice for DPS schemes in terms of the PAPR and BER performance. Its performance approaches that of conventional SPS systems. We also show that butterworth LPFs with low and even numbered orders are excellent choices for the proposed DPS schemes.

Our focus in this paper has been on considering the effect of the CFO and timing offset between two D/A or two A/D devices on the performance of linear equalisation. In a practical DPS system, there exist some other impairments (e.g. DC offset and I/Q imbalance). How to further develop joint mismatch calibration and compensation techniques will be interesting future research topics. To further reduce the required sampling rates of conversion devices, multiple pulse shaping transmission schemes satisfying ISI-free and CSI-free conditions and the corresponding equalisation methods may be further studied.

ACKNOWLEDGEMENTS

This work was supported by National Key R & D Program of China (Grant: 2018YFE0207500), Zhejiang Provincial Natural Science Foundation (Grant: LY22F010003 and LZ20F010004), the National Natural Science Foundation (Grant: 61871169 and 62071163), Project of Ministry of Science and Technology (Grant: D20011).

CONFLICT OF INTEREST

The authors declare no conflict of interest.

DATA AVAILABILITY STATEMENT

The data that support the findings of this study are available from the corresponding author upon reasonable request.

ORCID

Hang Li https://orcid.org/0000-0001-9996-9695

REFERENCES

1. Proakis, J., Salehi, M.: Digital Communications. 5th ed. McGraw-Hill, New York, NY (2008)
2. Yang, P., Xiao, Y., Xiao, M., Li, S.: 6G Wireless communications: Vision and potential techniques. IEEE Netw. 33(4), 70–75 (2019)
3. Dasalukunte, D., Owall, V., Rusek, F., Anderson, J.B.: Faster than Nyquist signaling: Algorithms to silicon. Springer International Publishing, Cham, Switzerland (2014)
4. Anderson, J.B., Rusek, F., Owall, V.: Faster-than-Nyquist signaling. Proc. IEEE 101(8), 1817–1830 (2013)

5. Ishihara, T., Sugiura, S.: Iterative frequency-domain joint channel estimation and data detection of faster-than-Nyquist signaling. IEEE Trans. Wireless Commun. 16(9), 6221–6231 (2017)
6. Yao, H., Wang, L., Wang, X., Zhou, L., Liu, Y.: The space-terrestrial integrated network : An overview. IEEE Commun. Mag. 56(9), 178–185 (2018)
7. Liu, J., Shi, Y., Fadlullah, Z.M., Kato, N.: Space-air-ground integrated network: A survey. IEEE Commun. Surv. Tutorials 20(4), 2714–2741 (2018)
8. Huq, K.M.S., Rodriguez, J.: Multiband and multichannel aggregation for high-speed wireless backhaul: challenges and solutions. In: Saidul Huq, K.M., Rodriguez, J., Backhauling/fronthauling for future wireless systems. 1st ed, John Wiley & Sons, Ltd, New York (2017)
9. Huang, X., Zhang, J.A., Liu, R.P., Guo, Y.J., Hanzo, L.: Airplane-aided integrated networking for 6g wireless: Will it work? IEEE Veh. Technol. Mag. 14(3), 84–91 (2019)
10. Rappaport, T.S., Heath Jr., R.W., Daniels, R.C., Murdock, J.: Millimeter wave wireless communications. Prentice-Hall, Englewood Cliffs, NJ (2014)
11. Li, X., et al.: 1-Tb/s millimeter-wave signal wireless delivery at D-band. J. Lightwave Technol. 37(1), 196–204 (2019)
12. Dan, I., Ducournau, G., Hisatake, S., Szriftgiser, P., Braun, R., Kallfass, I.: A terahertz wireless communication link using a superheterodyne approach. IEEE Trans. Terahertz Sci. Technol. 10(1), 32–43 (2020)
13. Standard High Speed ADC. Analog Device Inc. https://www.analog.com/en/products/ad9213.html#product-overview (2021). Accessed Jan 1, 2021
14. High Speed DAC. Analog Device Inc. https://www.analog.com/en/parametricsearch/10956#/ (2021). Accessed Jan 1, 2021
15. Buchwald, A.: High-speed time interleaved ADCs. IEEE Commun. Mag. 54(4), 71–77 (2016)
16. Hovakimyan, G., Hojabri, P., Martin, G.A., Satarzadeh, P.: Digital correction of time interleaved DAC mismatches. In: Proceedings of IEEE International Symposium on Circuits and Systems (ISCAS), pp. 1–5. IEEE, Piscataway, NJ, (2019)
17. Namgoong, W.: A channelized digital ultrawideband receiver. IEEE Trans. Wireless Commun. 2(3), 502–510 (2003)
18. Song, J., Tian, S., Hu, Y.H.: Analysis and correction of combined channel mismatch effects in frequency-interleaved ADCs. IEEE Trans. Circuits Syst. I Regul. Pap. 66(2), 655–668 (2019)
19. Huang, X., et al.: Dual pulse shaping transmission with complementary Nyquist pulses. In: Proceedings of IEEE 90th Vehicular Technology Conference (VTC), pp. 22–25. IEEE, Piscataway, NJ, (2019)
20. Zhang, H., et al.: A high-speed low-cost millimeter wave system with dual pulse shaping transmission and symbol rate equalization techniques. In: Proceedings of IEEE International Symposium on Circuits and Systems (ISCAS), pp. 26–29. IEEE, Piscataway, NJ, (2019)
21. Benvenuto, N., Ciccotosto, S., Tomasin, S.: Iterative block fractionally spaced nonlinear equalization for wideband channels. IEEE Wireless Commun. Lett. 4(5), 489–492 (2015)
22. Zhang, H., Huang, X., Zhang, J.A., Guo, Y.J.: Dual pulse shaping transmission and equalization for high-speed wideband wireless communication systems. IEEE Trans. Circuits Syst. I. Regul. Pap. 67(7), 2372–2382 (2020)
23. 'AD9739, RF DAC. Analog Device Inc. https://www.analog.com/media/en/technical-documentation/datasheets/AD9739.pdf (2021). Accessed Jan 1, 2021
24. Li, H., Wang, T.Q., Huang, X., Zhang, J.A., Guo, Y.J.: Low-complexity multiuser receiver for massive hybrid array mmWave communications. IEEE Trans. Commun. 67(5), 3512–3524 (2019)

How to cite this article: Li, H., Huang, X., Zhang, J.A., Zhang, H., Cheng, Z.: Dual pulse shaping transmission with sinc-function based complementary Nyquist pulses. IET Commun. 16, 2091–2104 (2022). https://doi.org/10.1049/cmu2.12463

APPENDIX A

The Derivation of $\mathbf{Y}(\omega, \tau)$

$Y(e^{j\omega})$ can be expressed as

$$\begin{aligned} Y(e^{j\omega}) =& Y_1(e^{j\omega}) + e^{-j\omega'} Y_2(e^{j\omega}) \\ =& \tilde{H}_1(e^{j\omega'}) S_1(e^{j2\omega'}) + \left(\tilde{H}_2(e^{j\omega'}) + \tilde{H}_e(e^{j\omega'})\right) S_2(e^{j2\omega'}) \\ &+ \tilde{W}(e^{j\omega}), \end{aligned} \tag{33}$$

where

$$\tilde{H}_1(e^{j\omega'}) = \frac{1}{T_s} \sum_{k=-\infty}^{+\infty} H_1\left(\frac{\omega'}{2\pi T_s} - \frac{k}{T_s}\right),$$

$$\tilde{H}_2(e^{j\omega'}) = \frac{1}{T_s} \sum_{k=-\infty}^{+\infty} H_2\left(\frac{\omega'}{2\pi T_s} - \frac{k}{T_s}\right),$$

$$\begin{aligned} \tilde{H}_e(e^{j\omega'}) =& \frac{1}{T_s} \sum_{k=-\infty}^{+\infty} 2j \sin\left(\pi k\tau - \frac{\omega'\tau}{2}\right) e^{j\left(\pi k\tau - \frac{\omega'\tau}{2}\right)} \\ &\times H_2\left(\frac{\omega'}{2\pi T_s} - \frac{k}{T_s}\right) \end{aligned}$$

and

$$\tilde{W}(e^{j\omega}) = \frac{1}{T_s} \sum_{k=-\infty}^{+\infty} W\left(\frac{\omega}{2\pi T_s} - \frac{k}{T_s}\right).$$

$\tilde{H}_1(e^{j\omega'})$, $\tilde{H}_2(e^{j\omega'})$, and $\tilde{W}(e^{j\omega})$ represent the digital DPS channel frequency responses without considering the timing offset between dual shaping pulses and frequency domain noise, respectively. $\tilde{H}_e(e^{j\omega'})$ represents the digital channel frequency-response error induced by the timing offset between dual shaping pulses.

Equation (34) can be expressed in matrix form as

$$\begin{aligned} \mathbf{Y}(\omega, \tau) =& \mathbf{H}(\omega', \tau)\mathbf{S}(\omega') + \mathbf{W}(\omega) = \left(\mathbf{H}(\omega', 0)\right. \\ &\left. + \mathbf{H}_e(\omega', \tau)\right) \mathbf{S}(\omega') + \mathbf{W}(\omega), 0 \le \omega < \pi \end{aligned} \tag{34}$$

where

$$\mathbf{S}(\omega') = \left[S_1(e^{j2\omega'}), S_2(e^{j2\omega'})\right]^T,$$

$$\mathbf{H}(\omega', 0) = \begin{bmatrix} \tilde{H}_1(e^{j\omega'}) & \tilde{H}_2(e^{j\omega'}) \\ \tilde{H}_1(e^{j(\omega'-\pi)}) & \tilde{H}_2(e^{j(\omega'-\pi)}) \end{bmatrix}$$

$$\mathbf{H}_e(\omega', \tau) = \begin{bmatrix} 0 & \tilde{H}_e(e^{j\omega'}) \\ 0 & \tilde{H}_e(e^{j(\omega'-\pi)}) \end{bmatrix}$$

and

$$\mathbf{W}(\omega) = \left[\tilde{W}(e^{j\omega}), \tilde{W}(e^{j(\omega-\pi)})\right]^T.$$